Is There Any Benefit of Coating Si Particles for a Negative Electrode Material for Lithium-Ion Batteries with Metal–Organic Frameworks? The Case of Aluminum Fumarate

Nassima Kana, Kaouther Touidjine, Sarah Olivier-Archambaud, Effrosyni Gkaniatsou, Michael Paris, Nicolas Dupré, Nicolas Gautier, Philippe Moreau, Clémence Sicard, Bernard Lestriez, et al.

▶ **To cite this version:**

Nassima Kana, Kaouther Touidjine, Sarah Olivier-Archambaud, Effrosyni Gkaniatsou, Michael Paris, et al.. Is There Any Benefit of Coating Si Particles for a Negative Electrode Material for Lithium-Ion Batteries with Metal–Organic Frameworks? The Case of Aluminum Fumarate. ACS Applied Energy Materials, inPress, 6 (18), pp.9218. 10.1021/acsaem.3c00658 . hal-04180595

HAL Id: hal-04180595
https://hal.science/hal-04180595v1

Submitted on 24 Aug 2023

HAL is a multi-disciplinary open access archive for the deposit and dissemination of scientific research documents, whether they are published or not. The documents may come from teaching and research institutions in France or abroad, or from public or private research centers.

L'archive ouverte pluridisciplinaire **HAL**, est destinée au dépôt et à la diffusion de documents scientifiques de niveau recherche, publiés ou non, émanant des établissements d'enseignement et de recherche français ou étrangers, des laboratoires publics ou privés.

Is there any benefit of coating Si particles for negative electrode material for Li-ion batteries with MOFs? The case of Al-fumarate

Nassima Kana,[1] Kaouther Touidjine,[1] Sarah Olivier-Archambaud,[1] Effrosyni Gkaniatsou,[2] Michael Paris,[1] Nicolas Dupré,[1] Nicolas Gautier,[1] Philippe Moreau,[1] Clémence Sicard,[2,3] Bernard Lestriez,[1] Thomas Devic[1*]*

[1] Nantes Université, CNRS, Institut des Matériaux de Nantes Jean Rouxel, IMN, F-44000 Nantes, France. E-mail : bernard.lestriez@cnrs-imn.fr, thomas.devic@cnrs-imn.fr

[2] Institut Lavoisier de Versailles, UMR 8180 CNRS UVSQ, Université Paris-Saclay, 45 avenue des Etats-Unis, 78035 Versailles, France.

[3] Institut universitaire de France (IUF).

KEYWORDS Li-ion batteries, Si electrodes, MOF, coating, Al fumarate

ABSTRACT Thanks to its high gravimetric and volumetric capacities, silicon is one of the most promising alternative to graphite for negative electrodes for Li-ion batteries. Its practical use is nevertheless hampered by it low capacity retention, resulting from its high volume variation upon cycling driving the formation of an unstable solid electrolyte interphase (SEI). Coatings of

Si particles with MOFs acting as artificial SEIs were recently reported, and found to lead to improved electrochemical performance in few cases. We here developed a room temperature route to coat Si particles with the Al-fumarate MOF (Al-fum), in conditions compatible to the aqueous formulation of state-of-the-art Si electrodes. Thanks to a variety of characterization techniques, including IR and solid-state NMR spectroscopies, powder X-ray diffraction and STEM-EDX analysis, we show that a layer of ca. 20 nm of MOF is grown at the surface of the Si particles. Nevertheless, such a coating does no translate in any major modification of the electrochemical performance when the Si particles are integrated in electrodes with a loading of practical interest (~2 mg_{Si} cm^{-2}). Post-mortem characterizations revealed that Al-fum, although being highly stable towards water, evolves in the standard LP30 electrolyte through a reaction with the PF_6^- anions. The MOF further reacts during the first electrochemical reduction, ultimately leading to Li aluminate phases, still located at the surface of the Si particles. Considering the growing interest of MOFs in the field of electrochemical energy storage, this let us conclude that there is probably a general need to more deeply and systematically evaluate the stability of MOFs towards battery electrolytes, and electrochemical processes.

Introduction

Among all potential active materials for the negative electrodes of Li-ion batteries (often quoted anode materials), silicon is considered as one of the most promising candidate because of its high gravimetric and volumetric capacities, about 3600 mAh g^{-1} and 2200 mAh cm^{-3}, respectively, as well as its low operation voltage (0.4 V vs. Li^+/Li), high natural abundancy and environmental benignity. However, during the lithiation (formation of Li_xSi, x~3.75), silicon undergoes an expansion of about 280% of its initial volume which induces numerous damages to the electrode

such as: (i) the pulverization of the Si particles, (ii) the loss of the cohesion of the electrode and of adhesion to the current collector and (iii) the formation of an unstable solid electrolyte interphase (SEI).[1,2] Points (i) and (ii) are typically addressed through the precise control of the Si particles size, shape and arrangement, and binder optimization, respectively. Regarding the SEI (point (iii)), electrolyte engineering (through the addition of reactive additives) is a common way to improve the composition and stability of the SEI,[3–6] even if the binder could also impact at least to some extent the nature of the silicon-electrolyte interphase.[7,8] Another strategy relies on the growth of a controlled coating on silicon, which will act as an artificial passivation layer, being either hard or soft to buffer or accommodate the volume expansion, respectively. Most studies have focused on metal oxides, carbons and conducting polymer coatings,[9–11] but coordination polymers are also of interest.[12] Metal alkoxides amorphous coordination polymers, such as alucone[13–16] or titanicone[17,18] (aluminum(III) and titanium(IV) glycerol derivatives, respectively), have been first proposed. Thin and conformal coatings were easily produced, but this method requires complex or costly deposition setups (Atomic or Molecular Layer Deposition).[19] Solution-based strategies were then proposed to grow amorphous coordination polymer coatings on Si/SiO_x particles, such as nickel trimesate,[20] zinc imidazolate,[21] and conducting iron polypyrrole.[22] The use of crystalline coordination polymers, especially Metal Organic Frameworks (MOFs), has also been proposed in the field of electrochemical energy storage.[23–27] Most studies focused on their use as active materials (either for the positive or negative electrodes of Li-ion batteries), in line with their controllable redox activity. Nevertheless, their tunable ordered microporosity also offers appealing prospects, such as (i) the storage of redox active materials to prevent leaching,[28] (ii) improved ionic transport when used as solid electrolytes,[29] or (iii) sieving properties to prevent redox shuttle when incorporated in/on

separators.[30] In this vein, there is a rising interest for the development of MOF coatings on Si and SiO_x active materials. The MOFs can be used either as sacrificial precursors to produce oxide or carbon coatings,[31–35] or be used in their native state. Their microporosity could potentially increase the adsorption of the salt and facilitate Li^+ ion transport, unlike other forms of coatings, while preventing the diffusion of other electrolyte components (solvents), and thus the massive formation of SEI. The first report on this topic dealt with the deposition of a MOF layer at the top of a pre-prepared Si electrode. This layer was found to improve in some cases the capacity retention, especially when small pores MOFs (ZIF-8, ZIF-67, ZIF = zinc imidazolate framework) or flexible MOFs (MIL-53(Al), MIL-53(Al)-NH_2, MIL = Materials Institute Lavoisier) were used.[36] This approach was recently extended to another MOF (HKUST-1)[37] and also applied to arrays of Si nanorods coated with ZIF-8.[38] All these MOFs are electrically insulating, potentially giving rise to charge transport limitation during cycling. To circumvent this problem, Nazir et al. reported the coating of Si nanoparticles by the semiconducting $Cu_3(HITP)_2$ (HITP = 2,3,6,7,10,11-hexaiminotriphenylene), from soluble reactants, in aqueous solution, followed by the formulation of the electrode.[39] Alternatively, Malik et al. showed that the simple addition of a MOF (here UiO-67, UiO = Universitetet i Oslo) during the preparation of Si electrodes could also improve the capacity retention to a certain extent, the MOF helping maintaining the porosity of the electrode upon cycling.[40] Whatever the selected MOF, even when an improvement of the electrochemical performance is detected, the evolution of the MOF at the molecular level, which could be induced either by the electrolyte or the electrochemical process (chemical or electrochemical transformation, respectively) remain scarcely investigated.[36,38,39] Broadly, the chemical stability of MOFs is a matter of concern since the seminal paper by Low at al. in 2009.[41] For example, the stability of MOF towards water is nowadays rather well understood and

controlled: strong cation-ligand bonds, obtained through the use of high-charge cations and/or basic ligands, lead to highly water stable MOFs.[41–45] To the best of our knowledge, there is currently no systematic study on the stability of MOF in standard anhydrous battery electrolytes, which typically contain polar complexing solvents and fluoride precursors, and thus no rationale linking the composition/structure of MOFs to their stability in these media.

We here focused our attention on the coating of Si particles in solution with MOF A-520, or Al-fum.[46] This MOF, formulated Al(OH)(fum) (fum = fumarate) is built up from chains of corner sharing AlO_6 octahedra connected through the dicarboxylate ligands and bridging inorganic OH groups to define diamond shaped channels of ~6 Å free diameter (Figure 1).[47] As most members of the Al-carboxylate family, this solid is highly stable towards water.[48] Furthermore, as all MIL-53 type MOFs, this solid presents a high structural flexibility,[49] at least when exposed to an isostatic pressure.[50] Such a solid should thus *a priori* be of interest to sustain the high mechanical constraints induced by the volume change of the electrode upon electrochemical cycling without damage, possibly leading to an improved capacity retention.

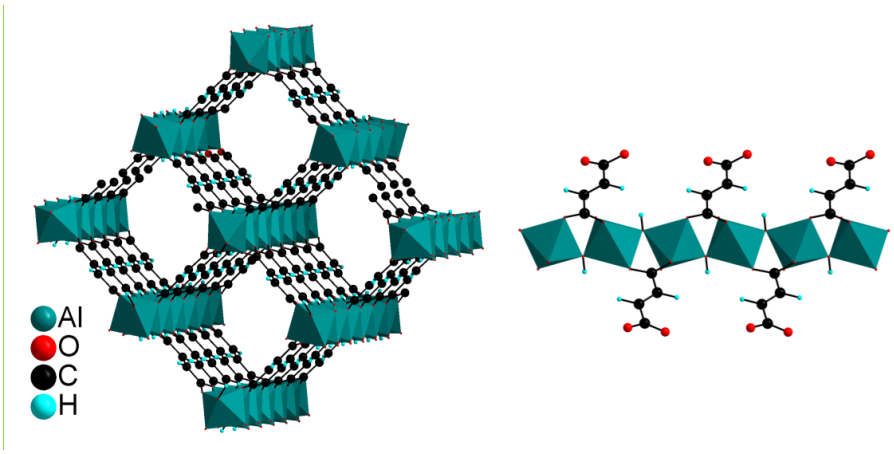

Figure 1. Crystal structure of A-520 or Al-fum. Left: view along the pore axis; right: view of the inorganic chain built up from AlO_6 octahedra connected through μ_2-OH bridges.

We here developed a synthetic procedure to prepare MOF-coated Si particles which align well with the state-of-the-art formulation of Si electrodes in aqueous medium[51] (room temperature, 2.5 < pH < 5, use of sodium aluminate to prevent the possible interference of the anion during the electrochemical process). The formation of the coating was assessed by a combination of techniques, including powder X-ray diffraction (PXRD), infrared (IR) spectroscopy, ^{27}Al solid-state nuclear magnetic resonance (NMR), thermogravimetric analyses (TGA) and scanning transmission electron microscopy coupled with energy dispersive X-ray spectroscopy (STEM-EDX). The effect of the coating on the electrochemical activity was evaluated on realistically loaded electrodes (m_{Si} > 2 mg cm^{-2}). The evolution of the MOF coated Si particles in the electrolyte and after electrochemical cycling was assessed, eventually showing that the MOF irreversibly transforms into most probably lithium aluminate phases.

Experimental Section

Materials

$NaAlO_2$, fumaric acid and polyacrylic acid (PAA, Mw = 450 000 g mol^{-1}) were purchased from Sigma-Aldrich and used as received. Silicon particles (particles size 150 nm, specific surface area 13.8 m²/g) was used as an active material. Ultrathin platelets of graphite consisting of short stacks of graphene sheets (xGnP graphene nanoplatelets grade M, thickness ~ 6−8 nm, D_{avg} =15 μm, XG Sciences) were used as a conductive additive.

Synthesis

Al-fum

123 mg (1.5 mmol) of $NaAlO_2$ was dissolved in 20 mL of water; 232 mg (2 mmol) of fumaric acid was added directly (as a powder) in this solution, and the mixture was stirred at room temperature for 48 hours. The resulting white solid was recovered by centrifugation (75000 rpm, 10 min), washed twice with water for 2 hours, and dried at 60°C for one night (Yield= 67.3 % based on ligand).

The amorphous coordination polymer *a*-Al-fumarate was prepared in the same conditions, except that the temperature was lowered to 0°C with an ice bath and that the reaction time was shortened to 4 hours.

Si/Al-fumarate composite

30.8 mg (0.38 mmol) of $NaAlO_2$ was dissolved in 5 mL of water; 250 mg (9 mmol) of silicon (particle size ~ 150 nm, surface area 13.8 m^2 g^{-1}) was added, and the suspension was stirred for 20 min. 58 mg (0.5 mmol) of fumaric acid was added and the mixture was stirred at room temperature for 48 hours. The resulting brown solid was recovered by centrifugation, washed twice with water for 2 hours, and dried at 60°C for one night.

The composite based on the amorphous coordination polymer *a*-Al-fum was prepared in the same conditions, except that the temperature was lowered to 0°C with an ice bath and that the reaction time was shortened to 4 hours.

Electrodes preparation

Electrode preparation: slurries were prepared from a mixture of silicon (coated or not), binder ($Li_{0.15}H_{0.85}$PAA), and conductive additive. The solid loading in the slurry was between 17 and 25%. The mixing was performed at 500 rpm for 1hr using a Fritsch Pulverisette 7 mixer with 3

silicon nitride balls (9.5 mm diameter). The slurries were tape cast onto a 28 μm thick copper foil (99.99%, MTI) by using an automatically moved Doctor blade (150 μm blade gap, speed 5 mm s^{-1}). The electrode film was firstly dried at room temperature overnight before being punched out into disks of 10 mm diameter. Finally, the obtained electrodes discs are dried at 100°C under vacuum for 2 hours to remove the residual water. The Si mass loading was varied from 1.5 to 2 mg cm-².

Characterizations

PXRD patterns were collected in a Bragg-Brentano mode with a Bruker D8 Advance diffractometer equipped with a Cu anode (λ = 1.5406 Å). Scanning electron microscopy (SEM) was carried out with a high-resolution JEOL JSM 7600F microscope, with back-scattered electrons detector and 5 kV as acceleration voltage. Samples were pasted on carbon tape and further coated with platinum to improve the surface electronic conductivity. STEM experiments were carried out using a Themis Z G3 Cs-probe corrected microscope from Thermo Fisher Scientific, operating at 80 kV. High-angle annular dark field (HAADF) images were acquired with a 30.5 mrad convergence angle and 50–200 mrad collection angles and EDX maps with 4 windowless silicon drift detectors (Super-X system). The solid was deposited onto a lacey carbon film supported by a copper grid. A vacuum transfer sample holder (GATAN 648) was used to prevent any air from contacting the reactive sample before its introduction into the microscope. Thermogravimetric analyses were performed by using a NETZSCH STA 449F3 Jupiter. 10-20 mg of product in an alumina crucible were necessary for the measurement. The measurements were performed under O_2 with a heating rate of 3°C min^{-1}, ranging from room temperature to 700°C for the MOF, and under air with a heating rate of 5°C min^{-1}, ranging from room temperature to 1000°C for the composites. ^{27}Al, ^{19}F, ^{7}Li magic angle spinning (MAS) NMR

spectra were recorded on a 500 MHz Bruker Avance III spectrometer (B_0 = 11.7 T) using a 2.5 mm probehead. The preparation of all samples but pristine Al-fum was performed in a glove box filled with Ar. After rinsing with 3-4 drops of dimethylcarbonate (DMC), the electrodes were dried in the glove box at room temperature for 12 hours, then scraped off the current collector and placed in the 2.5 mm diameter zirconia rotor. ^{7}Li MAS NMR spectra were acquired at a spinning frequency of 25 kHz with a single pulse sequence using a $\pi/2$ pulse and a recycle time of 40 s. ^{19}F MAS NMR spectra were acquired using a synchronized Hahn echo sequence with a one rotor period to discard the significant contribution from the probe signal at a spinning frequency of 25 kHz, and a recycle time of 30 s. Long recycle times were used to ensure quantitative measurements. ^{7}Li and ^{19}F chemical shifts were referenced to a 1M aqueous solution of LiCl and to solid state LiF (as a secondary reference at -204 ppm), respectively. For the ^{27}Al MAS spectra, a convergent DFS (Double Frequency Sweep)[52] pulse was used prior to the $\pi/12$ single pulse excitation of 2 µs length. The DFS pulse used induced a ^{27}Al signal enhancement by a factor 2.5 without distorting the line shapes. MAS frequency and recycle delay were set to 26 kHz and 1 s, respectively. ^{27}Al spectra were referenced against $Al(NO_3)_3$ aqueous solution. All spectra were analyzed using the DMfit software.[53] Infrared (IR) spectra were collected on a Bruker Alpha spectrometer in the attenuated total reflectance (ATR) mode between 400 and 4000 cm^{-1}. Electrochemical measurements were carried out in Swagelok type half-cells assembled with the dried Si-based composite electrodes (0.785 cm^2 disc). Two borosilicate glass-fiber (Whatman GF/D) and one polypropylene (PP) membrane (2500 grade, diam. = 13 mm, thickness 25 µm; Celgard®) were used as separators and were soaked in 300 µl of electrolyte consisting of LP30: 1M LiPF6 solution in EC-DMC (1:1) + 10 wt% FEC, or 1M LiTFSI solution in EC-DMC (1:1) + 10 wt% FEC. (TFSI = bis(trifluoromethanesulfonyl)imide). A lithium metal

foil was used as counter-electrode. The cells were assembled in the glove box under argon atmosphere. The cycling tests /were performed in galvanostatic mode over the potential window of 1-0.005 V versus Li^+/Li with a VMP multichannel electrochemical workstation (Bio-Logic). The current density was fixed at 90 mA g_{Si}^{-1} (C/40) for the first cycle, 180 mA g_{Si}^{-1} (C/20) for the 5 following cycles, and then at 360 mA g_{Si}^{-1} (C/10) for the 60 last cycles. Where C-rate was calculated based on a reversible theoretical silicon capacity of 3579 mAh g^{-1}. In order to evaluate the intrinsic electrochemical activity of Al-fum, some cycling experiments were also performed in Swagelok half cells assembled with the dried composite electrode which contains Al-fum as active material and TiN (particle diameter < 3µm, Sigma-Aldrich) as conductive additive mixed with water. The current density was set to 767 mA g_{MOF}^{-1}. For the stability tests in the electrolytes, 15 mg of Al-fum were dispersed in 1 mL of electrolyte for 4 days. The solids were recovered by centrifugation, washed with DMC, and dried at room temperature in a glove box filled with Ar.

Results and discussion

Synthesis and characterization

A pH of ~3 to 4 is known to be optimal for the formulation of Si electrodes in water, notably because it prevents the massive oxidation of the surface of the Si particles that could occur at higher pH.[51] This value aligns well with that used for the synthesis of Al-fum (pH~4), which is typically prepared in water from fumaric acid, $Al_2(SO_4)_3 \cdot nH_2O$ and NaOH at 60°C (BASF route).[46,47,54] We here first developed a slightly different reaction route, at a lower temperature (room temperature, RT), and using sodium aluminate ($NaAlO_2$) both as a base and aluminum

precursor. This latter allows avoiding the potential presence of remaining sulfate anions that might give rise to side electrochemical reactions. As evidenced by scanning electron microscopy (SEM), the MOF is isolated in the form of flake-like particles shorter than 100 nm (Figure S1). As shown Figure S2, the powder X-ray diffraction (PXRD) diagram of this product is in agreement with the pattern of standard Al-fum, and the calculated one. The width of the characteristic Bragg peaks is slightly larger than using the BASF route. This could arise either from a lower crystallinity of the MOF or from a smaller particle size. Nonetheless, Al-fum is well-known to give poorly crystallized particles, and a decrease of the crystallinity could be expected with the decrease of the reaction temperature from 60°C to RT. The infrared (IR) spectra of both solids are also similar, with the easily identified asymmetric and symmetric carboxylate vibration bands at 1620 and 1425 cm^{-1}, respectively, as well as the μ_2-OH vibration band at 3705 cm^{-1} (Figures 2a and S3). The ^{27}Al MAS NMR spectrum is consistent with the presence of corner-sharing AlO_6 octahedra (Figure 1c),[55] together with a minor amount of impurities, likely aluminum oxide/hydroxide. It is furthermore very close to that of Al-fum obtained through the BASF route,[47] confirming that both solids are identical. This similarity was further confirmed by thermogravimetric analysis (TGA) and nitrogen sorption isotherms measurements at 77 K (Figures S4 and S5, respectively). Especially, the N_2 sorption measurements revealed a type I isotherm characteristic of microporous materials and a BET surface area close to 1000 m^2/g, as expected for this MOF, confirming the effectiveness of our synthesis route.

In a second step, crystalline silicon particles (diameter ~ 150 nm, see Figure 3a) were added to the reaction mixture. The relative amount of reactants was adjusted to reach a final Si/MOF weight ratio in the range 5-10, so that the electrochemical gravimetric capacity of the derived

electrode is not too much impacted, while the MOF can be identified by standard characterization tools. The PXRD analysis of the composite (later labeled Si@Al-fum) first confirmed the formation of Al-fum: the main diffraction peaks at 10.3, 14.7 and 20.7° can be seen, together with an intense one at 28.4° characteristics of crystalline Si (Figure 2b). IR spectroscopy also confirmed the formation of the expected phase: the bands characteristics of the MOF are present, together with that of Si particles (Figure 2a). The ^{27}Al MAS NMR spectrum of Si@Al-fum compares well with the Al-fum one, although slightly broadened (Figure 2d). This can be associated with a lower crystallinity of Si@Al-fum. TGA under air was carried out to quantify the amount of MOF in the composite (Figure 2c). The experiment was first conducted on the pristine Si particles (brown curve): the weight increase, associated to the oxidation of Si to SiO_2, occurs above 500°C. It is thus safe to consider that for the Si@Al-fum composite, after the water departure at low temperature (<100°C), the composition on the first plateau (100-300°C, weight = 99%) should be Al(OH)(fum) + *n*Si. Considering that the combustion of Al-fum leading to the formation of Al_2O_3 occurs at 350-450°C, the composition at 500°C (weight = 90%) should be $1/2Al_2O_3$+ *n*Si. This leads to a molar ratio Si/Al around 35-40, corresponding to a Si/MOF weight ratio close to 7, in agreement with the introduced amounts. This value was further confirmed by nitrogen sorption experiments (see Figure S6). The composite Si@Al-fum was found to be microporous, with a BET surface area reaching 130 m^2 g^{-1}. Knowing that the surface area of the Si particles is negligible, the porosity arose exclusively from the MOF, which should then account for 130/1000 = 13 wt% of the composite, a value close to that obtained from TGA (14 wt%).

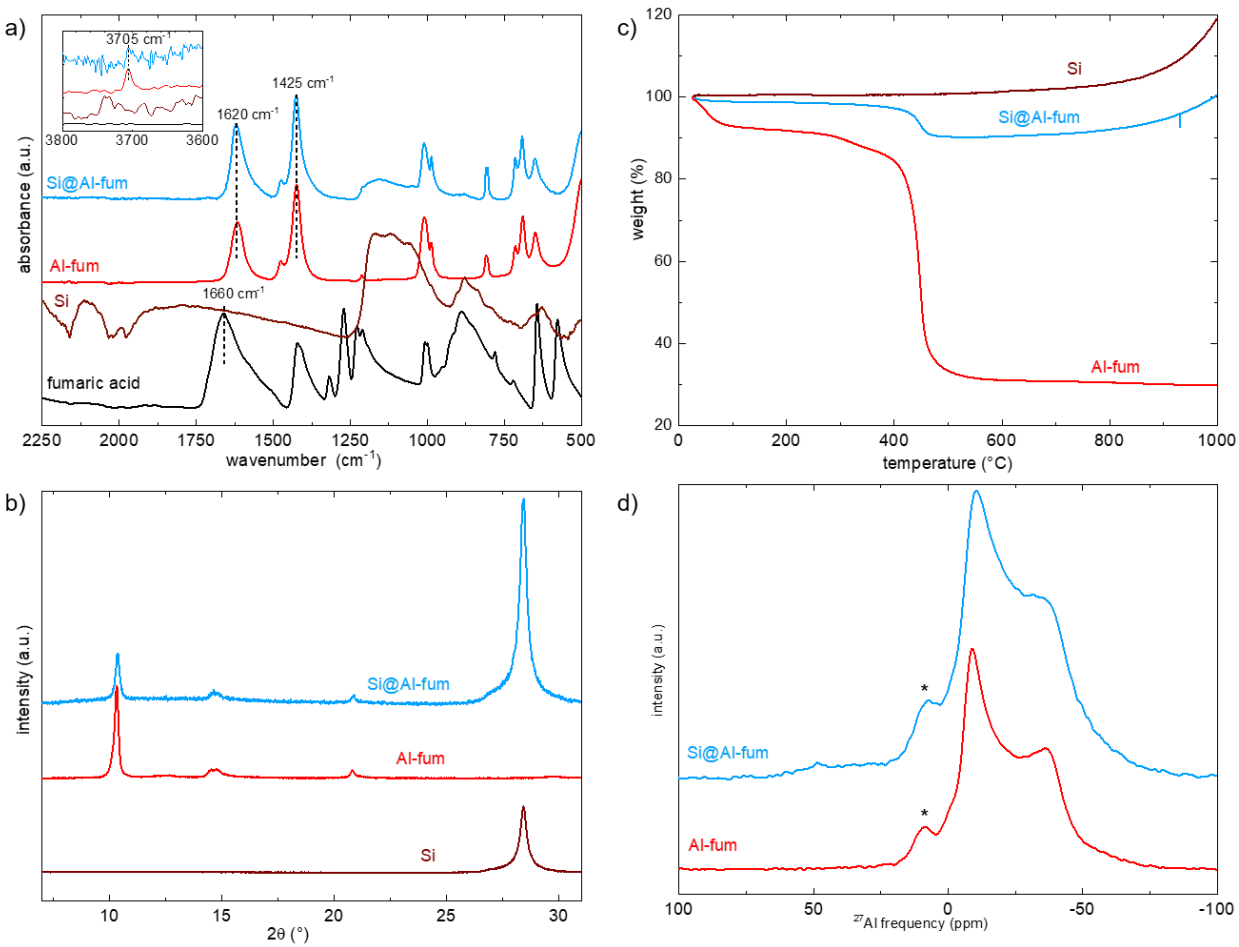

Figure 2. Characterization of the Si@Al-fum composite (blue), compared with pristine Si particles (brown) and pure Al-fum (red). a) IR spectra (inset: zoom on the O-H vibration zone); b) powder XRD patterns (λ = 1.5406 Å); c) TG analyses under air; d) ^{27}Al MAS NMR spectra (* = impurities).

This composite was further analyzed by scanning electron microscopy (SEM). As shown in Figure 3b, few aggregates of anisotropic particles, whose shape matches with that of Al-fum (see Figure S1), are visible, together with spherical particles of Si. If one compares with pristine Si (Figure 3a), these particles might be covered by a film, although the resolution of this analysis preclude any definitive answer.

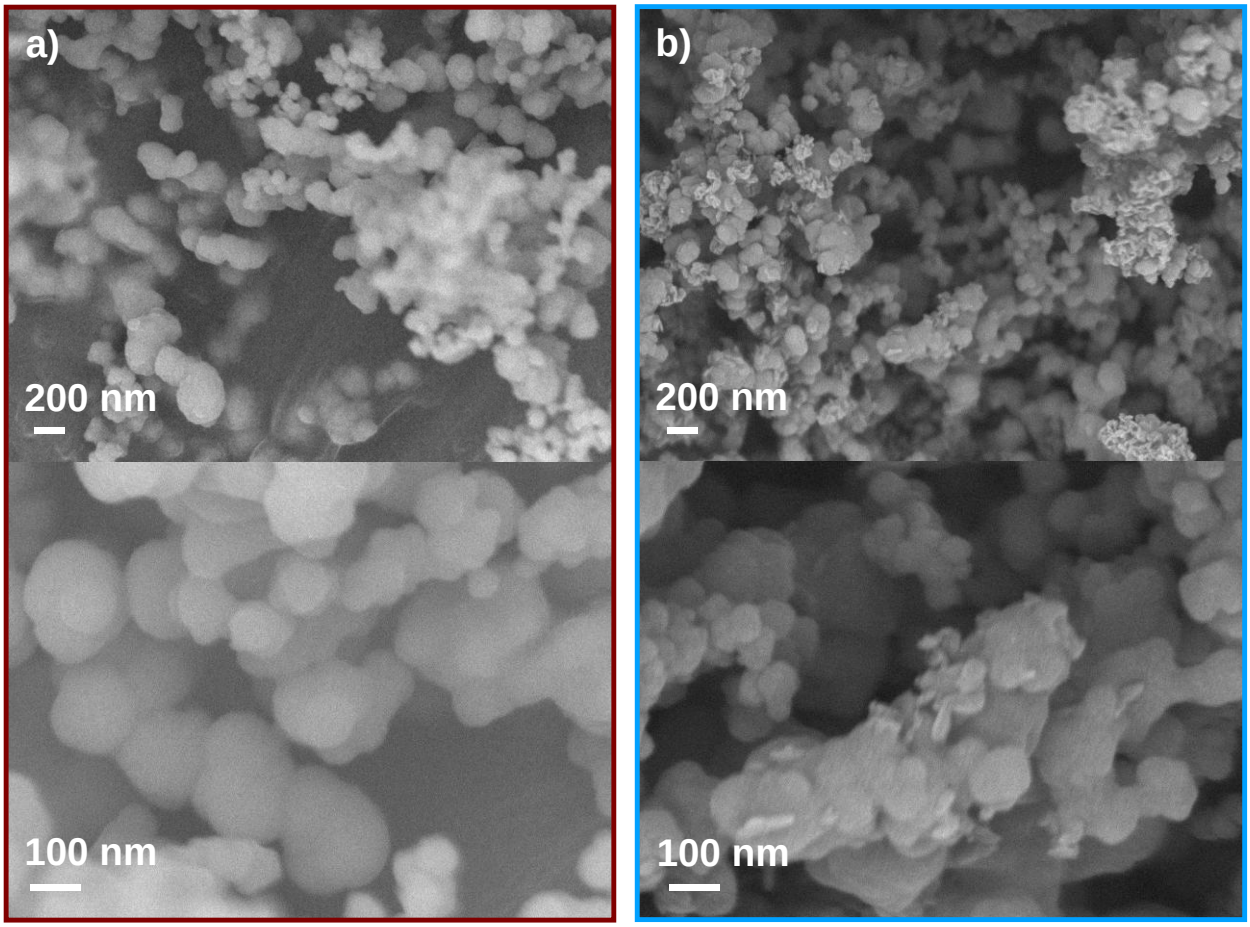

Figure 3. SEM pictures of a) pristine Si particles and b) Si@Al-fum composite. In the latter, both coated Si particles and aggregates of Al-fum particles are identified.

The fact that the Si particles are covered by Al-fum was ultimately evidenced by scanning transmission electron microscopy (STEM) analyses. The experiment was carried out on a complete electrode made of Si@Al-fum, polyacrylic acid (PAA) and conducting carbon additive in a 8:1:1 weight ratio (the full preparation will be described later). High-angle annular dark-field (HAADF) images of two representative areas are shown in Figure 4 (see Figure S7 for another area of interest). Round-shaped Si particles are easily identified, and appear to be covered by a thin layer of less dense material (this is more clearly visible on the left image, Figure 4). EDX mapping was further carried out. As expected, four main elements were detected: Si, Al, O and

C. Although belonging to Al-fum, C and O could not be considered as markers of the MOF, as they also belong to other components of the electrode (carbon additive and binder for C, binder and SiO_2 oxidation layer at the surface of Si for O). Hence, Al was considered as representative of the MOF. As hypothesized from the HAADF images, Al covers most of the surface of the Si particles (Figure 4, bottom). Note that although not exclusively representative of the MOF, the distribution of C to a certain extent, and mostly of O, also matches with that of Al (Figures S7). This unambiguously proves that Al-fum is grown on the Si particles, even if, as detected by MEB, isolated aggregates of Al-fum are also present. Although not fully conformal, this coating seems to cover most of the Si particles (Figure 4, left), with an averaged thickness of 20-30 nm (Figure 4, right).

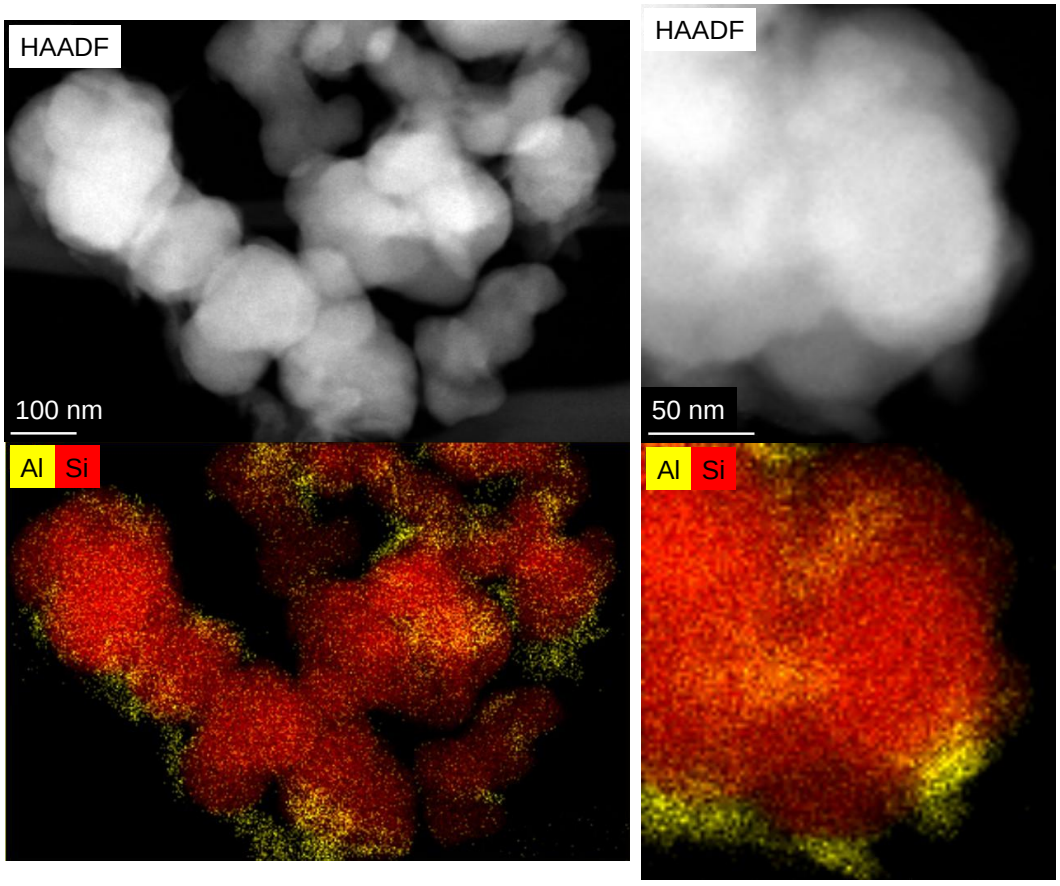

Figure 4. STEM-EDX pictures of electrodes based on the Si@Al-fum composite. Top: HAADF images; bottom: EDS mapping of Si and Al (other elements are shown in Figure S7).

Attempts to optimize the reaction conditions (temperature, concentration, Si/Al ratio, time…) to favor the growth of the MOF exclusively on the Si particles were carried out. When the reaction is performed at 0°C for a shorter time (4 instead of 48 hours), almost exclusively coated Si particles were observed by SEM (Figure S8). This was confirmed by a STEM-EDX analysis (Figure S9), which evidenced that Al is mainly located at the surface of the Si particles. The lower amount of organic matter in the composite was also evidenced by TGA: the weight loss associated with the combustion of the organic ligand reaches only 3% instead of ~10% for standard synthetic conditions (Figure S10). Nevertheless, PXRD indicated that this coating is amorphous (Figure S11). On the IR spectrum, characteristic bands of the carboxylate groups are visible at 1580 and 1425 cm^{-1} (Figure S12). Although these wavenumbers indicate that the carboxylic groups are effectively deprotonated, the asymmetric carboxylate vibration band is strongly shifted when compared to Al-fum ($\Delta \sim 40$ cm^{-1}), suggesting that the coordination polymer formed in these synthetic conditions is different. A signal is also seen at 3687 cm^{-1}, characteristic of an O-H vibration, but is again shifted when compared to standard, crystalline Al-fum (Δ~20 cm^{-1}). This solid, labeled *a*-Al-fum, was further prepared in the absence of Si particles. SEM indicated that it precipitates also in the form plate-like particles of ca 100 nm, a size and shape similar to that of Al-fum, suggesting that the result of the PXRD analysis is related to a loss of the long range order in *a*-Al-fum rather than to a reduction of the size of the crystalline domain. Al, C and O (no Na) were detected by SEM-EDX, confirming that this compound is an Al-fumarate coordination polymer (Figure S13). On the TGA curve, a continuous weight loss it observed at low temperature, followed by a major loss at 400-450°C,

associated with the combustion of the ligand and the formation of Al_2O_3. This weight loss is lower than that observed for Al-fumarate, indicating that *a*-Al-fum is richer in Al than Al-fum. Combining these results and IR spectroscopy, the tentative formula $AlO_x(OH)_y(fum)_z$, with $z < 0.5$ can be proposed. N_2 sorption experiment at 77 K indicates that this solid presents a rather modest microporosity (S_{BET}~ 90 m^2 g^{-1}) when compared to crystalline Al-fum. Although its structure is not fully defined, the composite Si@a-Al-fum was also considered in the electrochemical experiments.

Electrochemistry

Prior to the evaluation of the electrochemical performance of the Si-MOF composites, preliminary experiments were carried out to evaluate the electrochemical activity of Al-fum alone. Wang et al. already evaluated the activity of Al-fum in the potential range 0.01-3 V vs. Li^+/Li using electrodes made of Al-fum, acetylene black and polyvinylidene (PVDF).[56] They showed these electrodes could be cycled reversibly with a capacity of ca. 250 mAh g^{-1}, although this capacity is likely associated with an irreversible transformation of the MOF which occurred during the first cycles. We here evaluated the activity of Al-fum in the potential range of interest for Si anodes (0.005-1.000 V vs. Li^+/Li), with an electrolyte also suitable for such electrodes (LP30+10% FEC). In order to avoid any electrochemical activity arising from the carbonaceous additive at low potential, electrodes made of Al-fum and TiN were used. This latter is known to be a good electronic conductor, electrochemically inert, and thus suitable to study the electroactivity of minor components of battery electrodes.[57] Electrodes presenting various TiN:Al-fum weight compositions (100:0; 95:5, 80:20) were studied. A high amount of TiN was used to prevent any side effect related to the insulating character of the MOF. The current

density was set to ~770 mA g_{TiN}^{-1}, a value close to that used for the electrodes made of the Si@Al-fum composite (see below). Results are shown in Figure S15. During the first reduction down to 5 mV vs. Li^+/Li, a moderate capacity is detected (15-27 mAh g^{-1}), but the value does not correlate with the amount of Al-fum (the highest value is obtained for the electrode containing TiN only). No capacity (< 2 mAh g^{-1}) is detected during the first oxidation up to 1 V vs. Li^+/Li, as well as during the following cycles. We can thus conclude that Al-fum do not present any significant electrochemical activity in the standard conditions used to evaluate Si anodes.

Electrodes based on the Si-MOF composites were prepared using a recently optimized formulation, consisting of the Si-derived active material, graphene sheets as a conducting additive, and partially lithiated polyacrylic acid ($H_{0.85}Li_{0.15}PAA$) as a binder.[58] The mass loading was set to a value of practical interest (~ 2 mg_{Si} cm^{-2}). The composition of all the electrodes evaluated in this work is summarized in Table 1.

Table 1. Composition of the electrodes in weight %.

Formulation	Si	MOF	graphite	graphene	$H_{0.85}Li_{0.15}PAA$
ref. 1	80	-	-	10	10
ref. 2	70	-	10	10	10
Si@Al-fum	~70	~10	-	10	10
Si@*a*-Al-fum	~77	~3	-	10	10
Si+Al-fum_5	75	5	-	10	10
Si+Al-fum_10	70	10	-	10	10
Si+Al-fum_30	50	30	-	10	10

Four active materials were considered: pristine Si, Si@Al-fum, Si@*a*-Al-fum, and a physical mixture of Si and Al-fum with various weight ratios (Si+Al-fum_5, _10 and _30). This latter allowed potentially distinguishing the effect of the MOF coating and of the MOF aggregates in

the composite Si@Al-fum. The relative weight ratio of Si, carbon additive and binder is also known to affect the electrochemical performance of the electrode. Two reference electrodes made of pristine Si and identical amounts of carbon additive and binder (10 wt% each) were thus considered. Ref. 1 contains exclusively Si (80 wt%), while Ref. 2 contains 70 wt% of Si and 10 wt% of graphite, whose electrochemical contribution is negligible when compared to Si. Ref. 2 and Si@Al-fum thus present identical amount of Si (70 wt%).

The potential vs. capacity and the dQ/dV vs. potential curves for the first and second cycles are shown in Figure 5 for Ref. 1, Ref 2 and Si@Al-fum and Si@*a*-Al-fum and in Figure S16 for Si+Al-fum_5, _10 and _30. For the first cycle, the potential vs. capacity curves are similar whatever the composition of the electrodes, and characteristic of the activity of Si, with a plateau at 0.1 V vs. Li^+/Li during the first lithiation (Figure 5a, left). The polarization between the lithiation and delithiation curves are similar whatever the composition, suggesting the absence of any limitation of charge transport (electron and ion) by the MOF coating for most of the Si. Nevertheless, the irreversible capacities are also similar (and thus the coulombic efficiencies). This indicates that the coatings, both crystalline (Si@Al-fum) and amorphous (Si@*a*-Al-fum), do not limit the irreversible reduction of the electrolyte, hence that they do not act as efficient artificial passivation layers. Eventually, the initial capacity is slightly lower for the coated Si than for bare Si (~3500 vs 4000 mAh g_{Si}^{-1}), indicating that a small portion of the Si is not accessible in the electrodes based on coated particles, possibly that covered with an Al-fum (or *a*-Al-fum) layer too thick to allow charge transfer. In the second cycle, plateaus at 0.25 and 0.45 V vs. Li^+/Li are detected for Ref. 1, Ref 2 and Si@Al-fum (Figure 5a, right). These events are also clearly visible on the dQ/dV curves (Figure 5b, right) and are associated with the delithiation of amorphous Li_2Si (broad signal) and crystalline and amorphous $Li_{15}Si_4$ (sharp peak and broad

signal, respectively). The electrodes made of a physical mixture of Al-fum and Si present similar features (Figure S16).

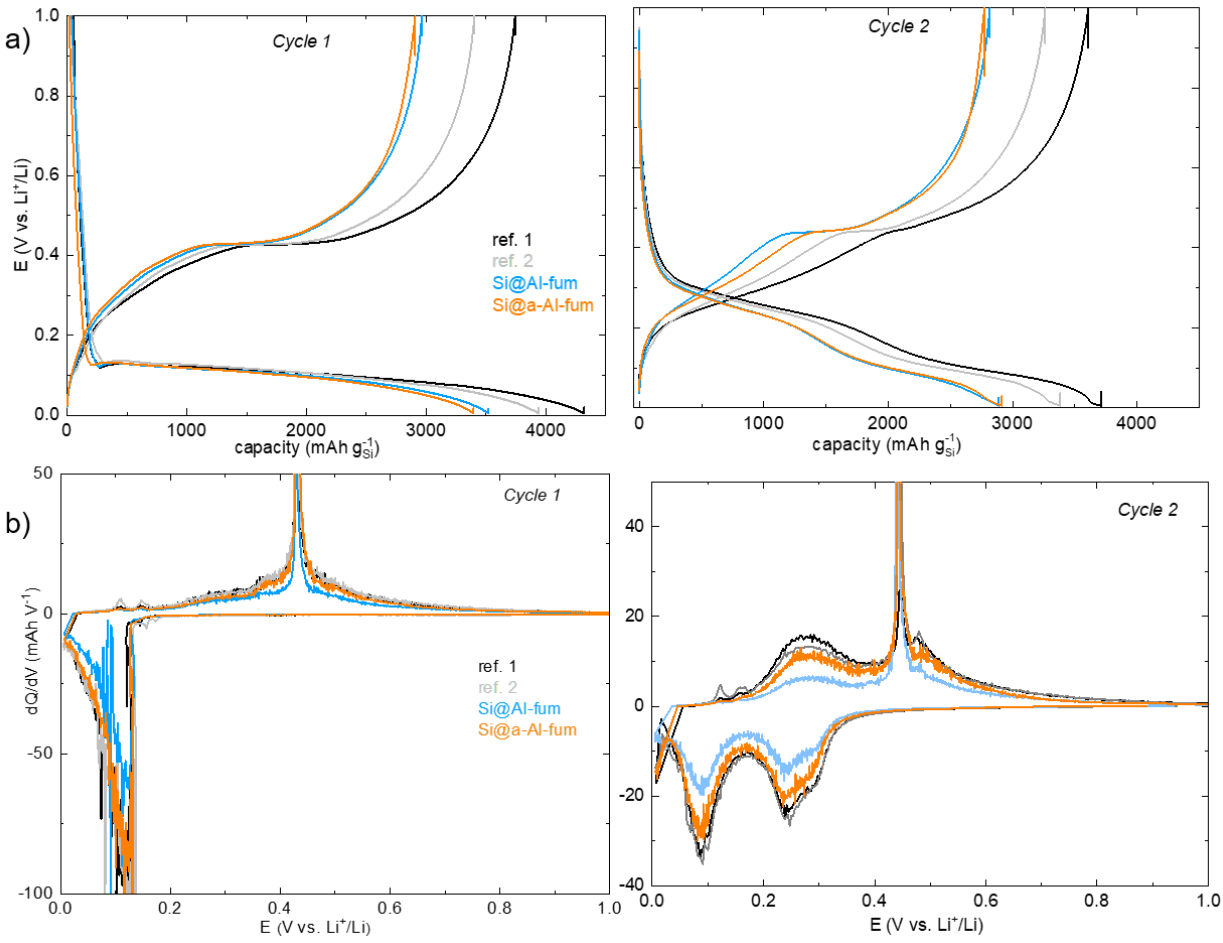

Figure 5. Electrochemical performance of the electrodes ref. 1, ref. 2, Si@Al-fum and Si@a-Al-fum (left: first cycle; right: second cycle). a) Potential vs. capacity curves; b) dQ/dV vs. potential curves.

The evolution of the capacity upon cycling, as well as the coulombic efficiency (CE), averaged on at least three independent cells, are shown Figure 6. Here again, no clear benefit in term of capacity retention associated with the MOF coatings, both crystalline and amorphous, is

detected. The capacity retention for Si@Al-fum and Si@a-Al-fum are rather similar, although slightly better for the amorphous coating after the first 10 cycles (but with a lower capacity). Both coated systems anyway present slightly lower capacities than that of both reference electrodes, as well as that containing a physical mixture of Si and Al-fum (Figure S17). The CE also evolves in a similar manner, reaching a value higher than 99% after 5 cycles whatever the composition of the electrodes, with the exception of Si+Al-fum_30, likely as a consequence of the very large amount of insulating MOF material in this electrode (30 wt%).

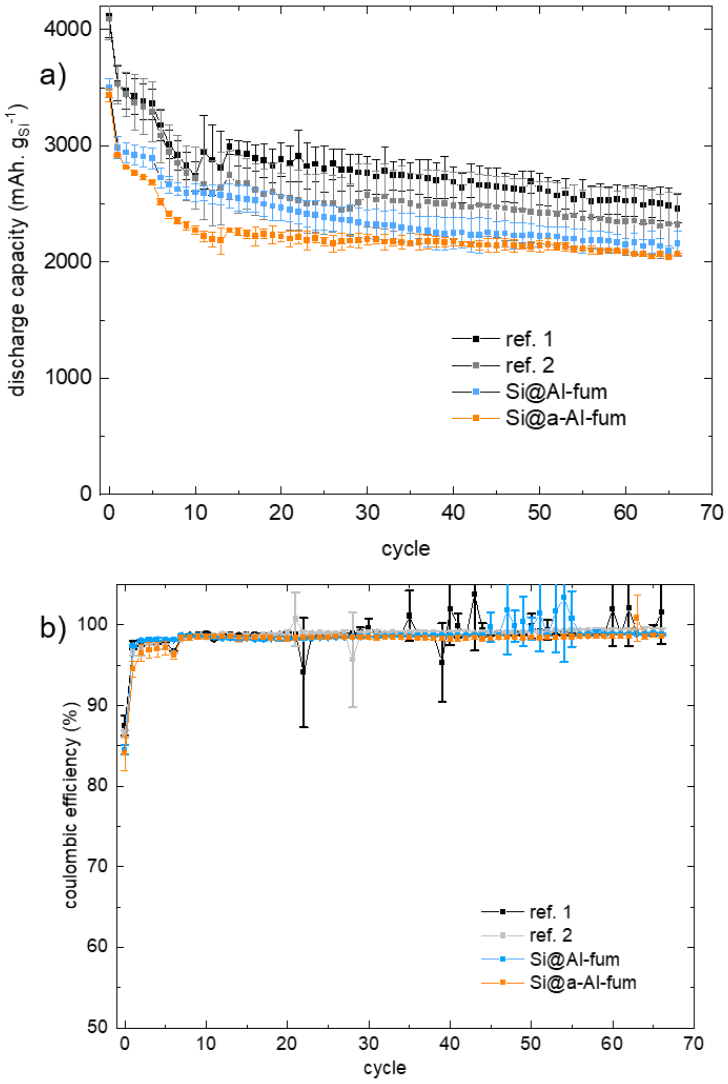

Figure 6. Evolution with cycling of the a) specific discharge capacities and b) coulombic efficiency (CE) for electrodes ref. 1, ref. 2, Si@Al-fum and Si@a-Al-fum.

To summarize, the absence of any major effect of the coating on the electrochemical performances of the Si electrodes, neither beneficial (higher CE during the first cycle, improvement of the capacity retention) nor detrimental (higher polarization) suggests that Al-fum does not act as an efficient artificial passivation layer. The question then arose whether the coating is maintained in the electrodes, and upon cycling. To answer this question, further characterizations were carried out on the complete electrodes (see below). It is also worth noting that the simple addition of Al-fum to the electrodes did not either significantly impact on their electrochemical behavior. This result differs from previous findings by Malik at al., who observed an improvement of the capacity retention when introducing a highly porous MOF (UiO-67) in the formulation with a similar Si:MOF weight ratio (~7:1).[40]

Evolution of the Al-fum coating

The stability of the Si@Al-fum coating was evaluated at three different stages: (i) on the pristine electrode, after the formulation, (ii) after exposure to electrolytes for 4 days, and (iii) after one electrochemical cycle. Various techniques were combined to probe the local environment of the components of the MOF (infrared and MAS NMR spectroscopies), the long-range order (PXRD), and the spatial distribution (STEM-EDX).

As described in the experimental section, the formulation of the electrodes consists in the dispersion of the Si@Al-fum particles in an aqueous, acidic (pH~3) medium, the mixing with the

binder and conducting additive by ball milling, the deposition of the resulting ink on a Cu current collector, and a drying step. The PXRD pattern of the electrode presents the expected diffraction peaks of Al-fum and Si (Figure S18), similarly to the pristine Si@Al-fum particles. Hence, the formulation step does not appear to damage the MOF, in line with the high stability of Al-carboxylate MOFs in aqueous media.[41,43] Eventually, STEM-EDX analysis confirmed that the MOFs is mostly localized at the surface of the Si particles (see above).

In order to evaluate the effect of the electrolyte, Al-fum and Si@Al-fum particles were suspended for 4 days in various solutions: a mixture of ethylene carbonate (EC) and dimethylcarbonate (DMC) in a 1:1 weight ratio, and the same mixture of solvents with 1 M $LiPF_6$ (LP30) or LiTFSI. The solids were then washed extensively with DMC to remove most of the salt, recovered by centrifugation and dried at room temperature. Al-fum was analyzed by infrared spectroscopy and PXRD in order to ensure a decent signal-to noise ratio, while ^{27}Al MAS NMR was carried out on the Si@Al-fum particles. The preparation and analyses were carried out under inert atmosphere (Ar) to prevent any side reaction with H_2O or O_2. The IR spectra are shown Figure 7a. In the presence of the solvents alone, no evolution of the band associated with Al-fum is detected. Only additional bands characteristic of residual carbonate solvents (1700-1800 cm^{-1}) are seen, together with a yet unidentified band at 1280 cm^{-1}. In the presence of 1 M LiTFSI, the spectrum is almost identical to that of the pristine Al-fum, indicating that the MOF is stable in this electrolyte. On the opposite, noticeable modifications are observed in LP30. Although the signal of the pristine Al-fum is still visible, peaks are broadened, and new bands appear. Especially, a shoulder at 1669 cm^{-1} is visible, indicating that a portion of Al-fum decomposed and that free carboxylic groups are formed. The band at ~3700 cm^{-1}, characteristic of the OH vibration, seems also to vanish in the presence of $LiPF_6$ (Figure 7, inset).

The same sample was subjected to ^{27}Al NMR (Figure 8b). After exposure to LP30, the shape of the signal evolves, suggesting a modification of the first coordination sphere of Al. Nevertheless, the chemical shift is still close to 0 ppm, indicating that Al^{3+} ions remain in an octahedral environment. All of this suggests that a reaction occurred between $LiPF_6$ and the MOF, possibly involving the reaction of PF_6^- anions with acidic OH groups, leading to the formation of HF ultimately reacting with the framework. Indeed, the substitution of OH by F in this material was shown to be possible (at least in aqueous medium).[54] The results of the PXRD analysis align well with this result: while the signal characteristics of the Al-fum is preserved for the solvents alone and in the presence of LiTFSI, a broadening of the signal is observed in LP30, together with a new peak at high angle (~28°) likely associated to an inorganic salt (Figure 7b). It should be recalled that Al-fum, as most M^{3+}-carboxylates, is considered to be a highly stable MOF, notably towards water.[41,43] Here, its limited stability might be related to the presence of frameworks acidic protons, which favor the degradation of PF_6^- and the formation of fluoride ions, ultimately able to form strong bonds with Al^{3+}.

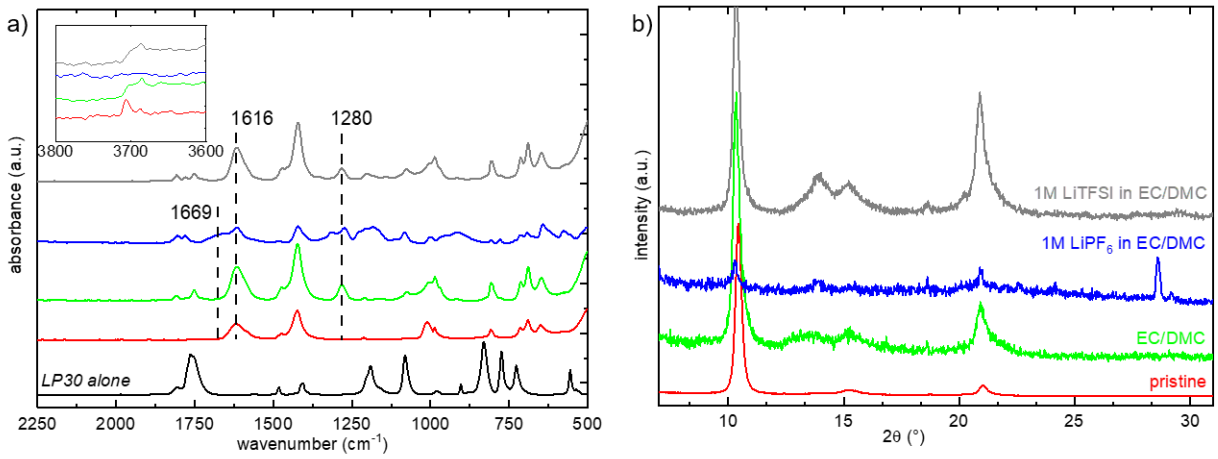

Figure 7. a) Infrared spectra and b) PXRD patterns and of Al-fum after being suspended for 4 days in EC/DMC, 1M $LiPF_6$ on EC/DMC (LP30), and 1 M LiTFSI in EC/DMC, compared to that of pristine Al-fum.

Ultimately, the electrodes were characterized after one electrochemical cycle in LP30. Again, the sample preparation, recovery, washing and analyses were performed in the absence of air to avoid any side reaction (see experimental section). First, in PXRD (Figure S18), the signal of the MOF completely vanished, indicating a complete loss of the long-range order. The electrode scratched from the Cu current was then studied by ^{7}Li, ^{19}F and ^{27}Al MAS NMR, and compared when possible to electrodes made of naked Si. Data are shown in Figure 8. The ^{7}Li spectrum of Si@Al-fum is almost identical to that obtained for pristine Si (Figure 8a), with a signal peak centered at ~0 ppm. As the measurements were performed at the end of the first Si delithiation process, only Li nuclei involved in the SEI are detected. This signal is associated with the presence of LiF, lithiated carbonaceous and/or organic products such as lithium carbonates and alkyl carbonates, typically observed when $LiPF_6$ electrolyte is used with carbonate solvents.[59–63] Nevertheless, the chemical shift for this isotope is known to be poorly sensitive to its surrounding, hence no further structural information can be gained from this analysis. ^{27}Al MAS NMR is much more informative (Figure 8b). When compared to Si@Al-fum particles, pristine (light blue) or suspended in LP30 (dark blue), the spectrum of the cycled electrode (green) shows marked differences. The signal centered at ca. -10 ppm characteristic of octahedrally coordinated Al^{3+} is still observed associated with strong broadening. More importantly, a new broad signal is clearly visible in the range 50-110 pm. A similar experiment carried out on the electrode after the first reduction (violet) showed that this new signal starts to appear during the first reduction. Such a chemical shift is characteristic of Al^{3+} in a tetrahedral coordination environment.[55] Al-

carboxylates usually adopt a 6-fold coordination (or 5-fold coordination when one of the ligand is labile enough to be thermally eliminated), and, to the best of our knowledge, no tetrahedral Al-carboxylate has been structurally characterized so far. This suggests that Al^{3+} ions eventually belong to aluminate (e.g. Li_5AlO_4 shows a signal centered at 92 ppm[64]) or fluoro-aluminate inorganic phases, or even mixed aluminosilicate phases. ^{19}F was used to try to answer this question (Figure 8c). The spectra of the electrodes made of pristine and coated Si particles are very similar, with the main signal at -206 ppm attributed to LiF, which is one of the main product of the SEI formed with the selected electrolyte. A minor additional signal is found at -75 ppm in the presence of the coating, but likely corresponds to other degradation products of the electrolyte such as $Li_xPO_yF_z$. Especially, no signal is detected in the range -155 to -175 ppm, where the characteristic signal of $AlF_{3-x}(OH)_x$ is expected.[65] There is thus no clear evidence of the massive formation of Al-F bonds.

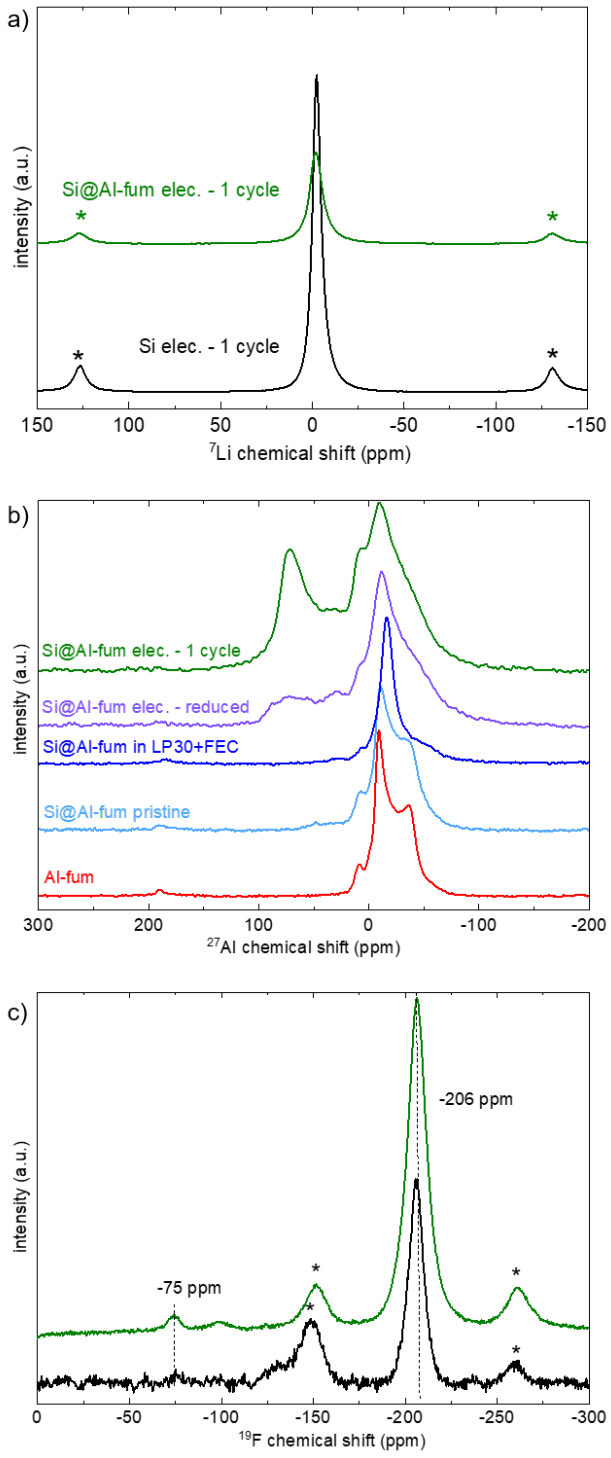

Figure 8. MAS NMR spectra of Si@Al-fum particles and of Si@Al-fum electrodes. a) ^{7}Li MAS NMR spectrum of a Si@Al-fum electrode after one cycle, compared to that obtained with naked Si particles; b) ^{27}Al MAS NMR spectra of Si@Al-fum particles suspended in electrolytes, and of

Si@Al-fum electrodes after one reduction and one complete cycle; c) ^{19}F MAS NMR spectrum of a Si@Al-fum electrode after one cycle, compared to that obtained with Si particles. * = rotation bands. Electrolyte: LP30 + 10wt% FEC.

STEM-EDX was eventually used to probe the location of this species. HAADF images of two representative areas are shown in Figure 9, together with the EDX mapping for Si and Al (see Figure S19 for F, O and C). Al species are clearly localized at the surface of the Si particles. The distribution of Al appears thus rather similar to that in pristine electrodes (Figure 3), although the layer appears to be thicker, and likely less dense. On the images and mappings (Figure 9), no dense particle of reduced Al (e.g. Al^0) was detected, suggesting that Al remains in the +3 oxidation state, in line with the ^{27}Al NMR analysis. No intimate mixing of Si and Al is either detected, suggesting that if any aluminosilicate phase is formed, it occurs only at a very small scale. Eventually, no obvious correlation is found between Al and F, supporting the fact that Al-F bonds are not present in large amount (Figure S19). The fumarate moieties could not be localized as their constitutive elements (C, O) are also present in the degradation products of the electrolyte and in the conducting additive.

Considering all these characterizations, we can hypothesize that the degradation of Al-fum occurs in two steps.

- a first chemical step, associated with its reaction with PF_6^- leading to the release of fumaric acid and possibly the formation of a minor amount of Al-F bonds

- a second electrochemical step, which do not involve the reduction of Al^{3+} to Al^0, but possibly the reduction of the ligand, leading to the formation of loosely packed lithium aluminates. Considering the little amount of MOF (molar Si/MOF ~35-40), such a reduction of the ligand,

which is expected to be irreversible,[66] will be undetectable in the electrochemical experiments. To conclude, even if Al-fum is irreversibly damaged, at least the inorganic part of the framework remained at the surface of the Si particles, and hence participates to the SEI. Nevertheless, such a layer does not lead to any beneficial effect in terms of electrochemical performance in half-cell.

In a last step, considering the better chemical stability of Al-MOF in the LiTFSI-containing electrolyte than in LP30, a preliminary electrochemical experiment was conducted using the Si@Al-fum electrodes and LiTFSI as a salt. As shown in Figure S20, the capacities are almost identical in both electrolytes for the first 20 cycles, while only a minor improvement is detected with LiTFSI upon longer cycling. Indeed, ^{27}Al MAS-NMR and STEM-EDX carried out after one cycle (Figures S21 and S22, respectively) showed a behavior similar to that observed in the presence of $LiPF_6$, namely an irreversible transformation of the MOF into species containing Al^{3+} in a tetrahedral coordination environment remaining at the surface of the Si particles. This suggests that the instability of Al-fum is not simply driven by the nature of the electrolyte, but also by the electrochemical process. Whatever the electrolyte, such a degradation has a minor impact on the electrochemical performance of the electrode in half-cells, at least in our experimental conditions.

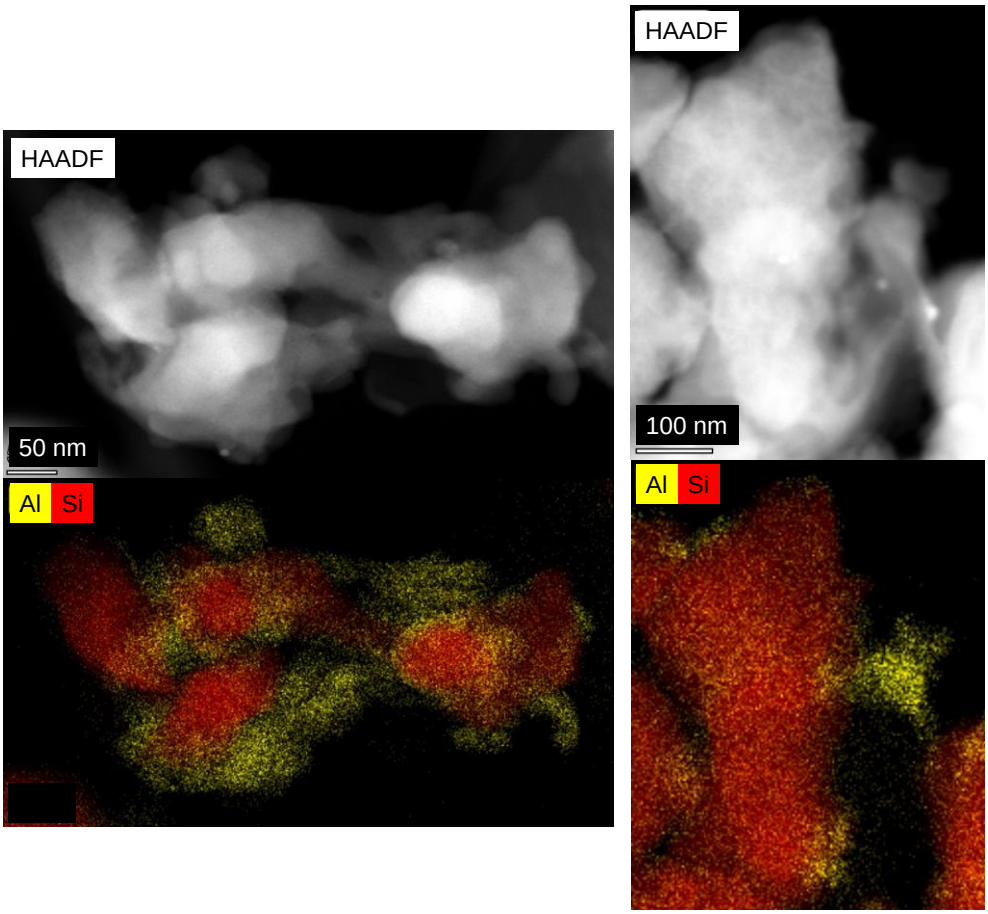

Figure 9. STEM-EDX pictures of electrodes based on the Si@Al-fum composite after one cycle (electrolyte: LP30 + 10wt% FEC). Top: HAADF images; bottom: EDS mapping of Si and Al (other elements are shown in Figure S19).

Conclusion

We have reported a procedure to coat Si particles with the porous Al-fum MOF in benign conditions (aqueous medium, room temperature). Although the layer is not as thin and conformal as alucone coatings obtained by MLD,[16] the MOF covers most of the Si particles. While initially constituted of crystalline Al-fum, the composition of this coating evolved when exposed to the

electrolyte LP30, and during the first electrochemical cycle towards what seems to be aluminate or mixed aluminate-silicate phases, but still localized at the surface of the Si particles. Even if the MOF appears more stable in the electrolyte based on LiTFSI rather than $LiPF_6$, a similar transformation is eventually observed after one electrochemical cycle. The resulting coating nevertheless does not affect significantly the electrochemical performance of the derived Si-electrodes in the tested conditions, neither positively, nor negatively. Improvements might arise from a better control of the thickness of the coating, and its uniformity, although the chemical transformation of the MOF into what seems to be lithium aluminates would still occur.

To conclude, with the ever-growing interest for MOF for electrochemical energy storage, there is probably an urgent need for a more systematic evaluation of their stability in the electrolytes and under electrochemical stress. This would be particularly relevant for "stable" MOF built up from high valence cations (charge = +3, +4), as these cations also form strong bonds with fluoride, an anion that is easily formed as a side product during electrochemical processes. As building (crystal) structure-properties relationships is an objective shared by many researchers in the field, such studies should be an important pre-requisite.

ASSOCIATED CONTENT

Supporting Information. Additional experimental data on Al-fum, Si@Al-fum and Si@a-Al-fum are provided, including SEM- and STEM-EDX, IR spectroscopy, PXRD, TGA, electrochemical curves and nitrogen sorption isotherms.

AUTHOR INFORMATION

Corresponding Author

* bernard.lestriez@cnrs-imn.fr, thomas.devic@cnrs-imn.fr

Author Contributions

NK, KT and SOA: synthesis and characterization of the composites, electrochemical evaluation; EG: synthesis and characterization of the MOF; MP and ND: NMR analysis; NG and PM: STEM-EDX analysis; CS and BL and TD: conceptualization and writing. The manuscript was written through contributions of all authors. All authors have given approval to the final version of the manuscript.

ACKNOWLEDGMENT

The authors thank S. Grolleau for the thermogravimetric and gas sorption analyses, and O. Stephan his help in the scanning electron microscopy experiments. The CNRS and Nantes Université are thanked for funding. Funding by the French Contrat Plan État-Région and the European Regional Development Fund of Pays de la Loire, the CIMEN Electron Microscopy Center in Nantes, is greatly acknowledged.

REFERENCES

(1) Kwon, T.; Choi, J. W.; Coskun, A. The Emerging Era of Supramolecular Polymeric Binders in Silicon Anodes. *Chem. Soc. Rev.* **2018**, *47* (6), 2145–2164. https://doi.org/10.1039/C7CS00858A.

(2) Guo, J.; Dong, D.; Wang, J.; Liu, D.; Yu, X.; Zheng, Y.; Wen, Z.; Lei, W.; Deng, Y.; Wang, J.; Hong, G.; Shao, H. Silicon-Based Lithium Ion Battery Systems: State-of-the-Art from Half and Full Cell Viewpoint. *Adv. Funct. Mater.* **2021**, *31* (34), 2102546. https://doi.org/10.1002/adfm.202102546.

(3) Hu, Z.; Zhao, L.; Jiang, T.; Liu, J.; Rashid, A.; Sun, P.; Wang, G.; Yan, C.; Zhang, L. Trifluoropropylene Carbonate-Driven Interface Regulation Enabling Greatly Enhanced Lithium Storage Durability of Silicon-Based Anodes. *Adv. Funct. Mater.* **2019**, *29* (45), 1906548. https://doi.org/10.1002/adfm.201906548.

(4) Jin, Y.; Kneusels, N.-J. H.; Marbella, L. E.; Castillo-Martínez, E.; Magusin, P. C. M. M.; Weatherup, R. S.; Jónsson, E.; Liu, T.; Paul, S.; Grey, C. P. Understanding Fluoroethylene Carbonate and Vinylene Carbonate Based Electrolytes for Si Anodes in Lithium Ion Batteries with NMR Spectroscopy. *J. Am. Chem. Soc.* **2018**, *140* (31), 9854–9867. https://doi.org/10.1021/jacs.8b03408.

(5) Guo, L.; Huang, F.; Cai, M.; Zhang, J.; Ma, G.; Xu, S. Organic–Inorganic Hybrid SEI Induced by a New Lithium Salt for High-Performance Metallic Lithium Anodes. *ACS Appl. Mater. Interfaces* **2021**, *13* (28), 32886–32893. https://doi.org/10.1021/acsami.1c04788.

(6) Schneier, D.; Shaham, Y.; Ardel, G.; Burstein, L.; Kamir, Y.; Peled, E. Elucidation of the Spontaneous Passivation of Silicon Anodes in Lithium Battery Electrolytes. *J. Electrochem. Soc.* **2019**, *166* (16), A4020–A4024. https://doi.org/10.1149/2.1081915jes.

(7) Han, L.; Liu, T.; Sheng, O.; Liu, Y.; Wang, Y.; Nai, J.; Zhang, L.; Tao, X. Undervalued Roles of Binder in Modulating Solid Electrolyte Interphase Formation of Silicon-Based Anode Materials. *ACS Appl. Mater. Interfaces* **2021**, *13* (38), 45139–45148. https://doi.org/10.1021/acsami.1c13971.

(8) Huet, L.; Moreau, P.; Dupré, N.; Devic, T.; Roué, L.; Lestriez, B. Nanoscale Morphological Characterization of Coordinated Binder and Solid Electrolyte Interphase in

Silicon-Based Electrodes for Li-Ion Batteries. *Small Methods* **2022**, *6* (10), 2200827. https://doi.org/10.1002/smtd.202200827.

(9) Luo, W.; Chen, X.; Xia, Y.; Chen, M.; Wang, L.; Wang, Q.; Li, W.; Yang, J. Surface and Interface Engineering of Silicon-Based Anode Materials for Lithium-Ion Batteries. *Adv. Energy Mater.* **2017**, *7* (24), 1701083. https://doi.org/10.1002/aenm.201701083.

(10) Rage, B.; Delbegue, D.; Louvain, N.; Lippens, P.-E. Engineering of Silicon Core-Shell Structures for Li-Ion Anodes. *Chem. Eur. J.* **2021**, *27* (66), 16275–16290. https://doi.org/10.1002/chem.202102470.

(11) Xu, K.; Liu, X.; Guan, K.; Yu, Y.; Lei, W.; Zhang, S.; Jia, Q.; Zhang, H. Research Progress on Coating Structure of Silicon Anode Materials for Lithium-Ion Batteries. *ChemSusChem* **2021**, *14* (23), 5135–5160. https://doi.org/10.1002/cssc.202101837.

(12) Devic, T.; Lestriez, B.; Roué, L. Silicon Electrodes for Li-Ion Batteries. Addressing the Challenges through Coordination Chemistry. *ACS Energy Lett.* **2019**, *4* (2), 550–557. https://doi.org/10.1021/acsenergylett.8b02433.

(13) Piper, D. M.; Travis, J. J.; Young, M.; Son, S.-B.; Kim, S. C.; Oh, K. H.; George, S. M.; Ban, C.; Lee, S.-H. Reversible High-Capacity Si Nanocomposite Anodes for Lithium-Ion Batteries Enabled by Molecular Layer Deposition. *Adv. Mater.* **2014**, *26* (10), 1596–1601. https://doi.org/10.1002/adma.201304714.

(14) Ma, Y.; Martinez de la Hoz, J. M.; Angarita, I.; Berrio-Sanchez, J. M.; Benitez, L.; Seminario, J. M.; Son, S.-B.; Lee, S.-H.; George, S. M.; Ban, C.; Balbuena, P. B. Structure and

Reactivity of Alucone-Coated Films on Si and LixSiy Surfaces. *ACS Appl. Mater. Interfaces* **2015**, *7* (22), 11948–11955. https://doi.org/10.1021/acsami.5b01917.

(15) Son, S.-B.; Wang, Y.; Xu, J.; Li, X.; Groner, M.; Stokes, A.; Yang, Y.; Cheng, Y.-T.; Ban, C. Systematic Investigation of the Alucone-Coating Enhancement on Silicon Anodes. *ACS Appl. Mater. Interfaces* **2017**, *9* (46), 40143–40150. https://doi.org/10.1021/acsami.7b08960.

(16) He, Y.; Piper, D. M.; Gu, M.; Travis, J. J.; George, S. M.; Lee, S.-H.; Genc, A.; Pullan, L.; Liu, J.; Mao, S. X.; Zhang, J.-G.; Ban, C.; Wang, C. In Situ Transmission Electron Microscopy Probing of Native Oxide and Artificial Layers on Silicon Nanoparticles for Lithium Ion Batteries. *ACS Nano* **2014**, *8* (11), 11816–11823. https://doi.org/10.1021/nn505523c.

(17) Huertas, Z. C.; Settipani, D.; Flox, C.; Morante, J. R.; Kallio, T.; Biendicho, J. J. High Performance Silicon Electrode Enabled by Titanicone Coating. *Sci Rep* **2022**, *12* (1), 137. https://doi.org/10.1038/s41598-021-04105-x.

(18) Fang, J.-B.; Chang, S.; Ren, Q.; Zi, T.; Wu, D.; Li, A.-D. Tailoring Stress and Ion-Transport Kinetics via a Molecular Layer Deposition-Induced Artificial Solid Electrolyte Interphase for Durable Silicon Composite Anodes. *ACS Appl. Mater. Interfaces* **2021**, *13* (27), 32520–32530. https://doi.org/10.1021/acsami.1c07572.

(19) Ban, C.; George, S. M. Molecular Layer Deposition for Surface Modification of Lithium-Ion Battery Electrodes. *Adv. Mater. Interfaces* **2016**, *3* (21), 1600762. https://doi.org/10.1002/admi.201600762.

(20) Huang, W.; Wang, W.; Wang, Y.; Qu, Q.; Jin, C.; Zheng, H. Overcoming the Fundamental Challenge of PVDF Binder Use with Silicon Anodes with a Super-Molecular Nano-Layer. *J. Mater. Chem. A* **2021**, *9* (3), 1541–1551. https://doi.org/10.1039/D0TA10301B.

(21) Yu, Y.; Yue, C.; Han, Y.; Zhang, C.; Zheng, M.; Xu, B.; Lin, S.; Li, J.; Kang, J. Si Nanorod Arrays Modified with Metal–Organic Segments as Anodes in Lithium Ion Batteries. *RSC Adv.* **2017**, *7* (85), 53680–53685. https://doi.org/10.1039/C7RA10905A.

(22) Zhou, J.; Qian, T.; Wang, M.; Xu, N.; Zhang, Q.; Li, Q.; Yan, C. Core–Shell Coating Silicon Anode Interfaces with Coordination Complex for Stable Lithium-Ion Batteries. *ACS Appl. Mater. Interfaces* **2016**, *8* (8), 5358–5365. https://doi.org/10.1021/acsami.5b12392.

(23) Zhou, J.; Wang, B. Emerging Crystalline Porous Materials as a Multifunctional Platform for Electrochemical Energy Storage. *Chem. Soc. Rev.* **2017**, *46* (22), 6927–6945. https://doi.org/10.1039/C7CS00283A.

(24) Xu, Y.; Li, Q.; Xue, H.; Pang, H. Metal-Organic Frameworks for Direct Electrochemical Applications. *Coord. Chem. Rev.* **2018**, *376*, 292–318. https://doi.org/10.1016/j.ccr.2018.08.010.

(25) Wang, Z.; Tao, H.; Yue, Y. Metal-Organic-Framework-Based Cathodes for Enhancing the Electrochemical Performances of Batteries: A Review. *ChemElectroChem* **2019**, *6* (21), 5358–5374. https://doi.org/10.1002/celc.201900843.

(26) Liu, J.; Xie, D.; Shi, W.; Cheng, P. Coordination Compounds in Lithium Storage and Lithium-Ion Transport. *Chem. Soc. Rev.* **2020**, *49* (6), 1624–1642. https://doi.org/10.1039/C9CS00881K.

(27) Schneemann, A.; Dong, R.; Schwotzer, F.; Zhong, H.; Senkovska, I.; Feng, X.; Kaskel, S. 2D Framework Materials for Energy Applications. *Chem. Sci.* **2021**, *12* (5), 1600–1619. https://doi.org/10.1039/D0SC05889K.

(28) Demir-Cakan, R.; Morcrette, M.; Nouar, F.; Davoisne, C.; Devic, T.; Gonbeau, D.; Dominko, R.; Serre, C.; Férey, G.; Tarascon, J.-M. Cathode Composites for Li-S Batteries via the Use of Oxygenated Porous Architectures. *J. Am. Chem. Soc.* **2011**, *133*, 16154–16160.

(29) Zhao, R.; Wu, Y.; Liang, Z.; Gao, L.; Xia, W.; Zhao, Y.; Zou, R. Metal–Organic Frameworks for Solid-State Electrolytes. *Energy Environ. Sci.* **2020**, *13* (8), 2386–2403. https://doi.org/10.1039/D0EE00153H.

(30) Chu, Z.; Gao, X.; Wang, C.; Wang, T.; Wang, G. Metal–Organic Frameworks as Separators and Electrolytes for Lithium–Sulfur Batteries. *J. Mater. Chem. A* **2021**, *9* (12), 7301–7316. https://doi.org/10.1039/D0TA11624F.

(31) Han, Y.; Qi, P.; Feng, X.; Li, S.; Fu, X.; Li, H.; Chen, Y.; Zhou, J.; Li, X.; Wang, B. In Situ Growth of MOFs on the Surface of Si Nanoparticles for Highly Efficient Lithium Storage: Si@MOF Nanocomposites as Anode Materials for Lithium-Ion Batteries. *ACS Appl. Mater. Interfaces* **2015**, *7* (4), 2178–2182. https://doi.org/10.1021/am5081937.

(32) Liu, N.; Liu, J.; Jia, D.; Huang, Y.; Luo, J.; Mamat, X.; Yu, Y.; Dong, Y.; Hu, G. Multi-Core Yolk-Shell like Mesoporous Double Carbon-Coated Silicon Nanoparticles as Anode Materials for Lithium-Ion Batteries. *Energy Storage Mater.* **2019**, *18*, 165–173. https://doi.org/10.1016/j.ensm.2018.09.019.

(33) Majeed, M. K.; Ma, G.; Cao, Y.; Mao, H.; Ma, X.; Ma, W. Metal–Organic Frameworks-Derived Mesoporous Si/SiOx@NC Nanospheres as a Long-Lifespan Anode Material for Lithium-Ion Batteries. *Chem. Eur. J.* **2019**, *25* (51), 11991–11997. https://doi.org/10.1002/chem.201903043.

(34) Wang, K.; Pei, S.; He, Z.; Huang, L.; Zhu, S.; Guo, J.; Shao, H.; Wang, J. Synthesis of a Novel Porous Silicon Microsphere@carbon Core-Shell Composite via in Situ MOF Coating for Lithium Ion Battery Anodes. *Chem. Eng. J.* **2019**, *356*, 272–281. https://doi.org/10.1016/j.cej.2018.09.027.

(35) Zou, W.; Li, T.; Yao, Z.; Fan, M.; Ma, T. A Comprehensive Study on ZIF-8/SiOx/ZIF-8 Core-Shell Composite as High-Stable Anode Material for Lithium-Ion Batteries. *J. Electroanal. Chem.* **2022**, *912*, 116258. https://doi.org/10.1016/j.jelechem.2022.116258.

(36) Han, Y.; Qi, P.; Zhou, J.; Feng, X.; Li, S.; Fu, X.; Zhao, J.; Yu, D.; Wang, B. Metal–Organic Frameworks (MOFs) as Sandwich Coating Cushion for Silicon Anode in Lithium Ion Batteries. *ACS Appl. Mater. Interfaces* **2015**, *7* (48), 26608–26613. https://doi.org/10.1021/acsami.5b08109.

(37) Shin, J.; Kim, T.-H.; Kang, H.; Cho, E. Epitaxial Metal–Organic Framework for Stabilizing the Formation of a Solid Electrolyte Interphase on the Si Anode of a Lithium-Ion Battery. *ACS Sustainable Chem. Eng.* **2022**, *10* (32), 10615–10626. https://doi.org/10.1021/acssuschemeng.2c02337.

(38) Yu, Y.; Yue, C.; Lin, X.; Sun, S.; Gu, J.; He, X.; Zhang, C.; Lin, W.; Lin, D.; Liao, X.; Xu, B.; Wu, S.; Zheng, M.; Li, J.; Kang, J.; Lin, L. ZIF-8 Cooperating in TiN/Ti/Si Nanorods as

Efficient Anodes in Micro-Lithium-Ion-Batteries. *ACS Appl. Mater. Interfaces* **2016**, *8* (6), 3992–3999. https://doi.org/10.1021/acsami.5b11287.

(39) Nazir, A.; Le, H. T. T.; Kasbe, A.; Park, C.-J. Si Nanoparticles Confined within a Conductive 2D Porous Cu-Based Metal–Organic Framework (Cu3(HITP)2) as Potential Anodes for High-Capacity Li-Ion Batteries. *Chem. Eng. J.* **2021**, *405*, 126963. https://doi.org/10.1016/j.cej.2020.126963.

(40) Malik, R.; Loveridge, Melanie. J.; Williams, L. J.; Huang, Q.; West, G.; Shearing, P. R.; Bhagat, R.; Walton, R. I. Porous Metal–Organic Frameworks for Enhanced Performance Silicon Anodes in Lithium-Ion Batteries. *Chem. Mater.* **2019**, *31* (11), 4156–4165. https://doi.org/10.1021/acs.chemmater.9b00933.

(41) Low, J. J.; Benin, A. I.; Jakubczak, P.; Abrahamian, J. F.; Faheem, S. A.; Willis, R. R. Virtual High Throughput Screening Confirmed Experimentally: Porous Coordination Polymer Hydration. *J. Am. Chem. Soc.* **2009**, 15834–15842. https://doi.org/10.1021/ja9061344.

(42) Devic, T.; Serre, C. High Valence 3p and Transition Metals Based MOFs. *Chem. Soc. Rev.* **2014**, *43*, 6097–6115.

(43) Leus, K.; Bogaerts, T.; De Decker, J.; Depauw, H.; Hendrickx, K.; Vrielinck, H.; Van Speybroeck, V.; Van Der Voort, P. Systematic Study of the Chemical and Hydrothermal Stability of Selected "Stable" Metal Organic Frameworks. *Micro. Meso. Mater.* **2016**, *226*, 110–116. https://doi.org/10.1016/j.micromeso.2015.11.055.

(44) Liu, X.; Wang, X.; Kapteijn, F. Water and Metal–Organic Frameworks: From Interaction toward Utilization. *Chem. Rev.* **2020**, *120* (16), 8303–8377. https://doi.org/10.1021/acs.chemrev.9b00746.

(45) Moumen, E.; Assen, A. H.; Adil, K.; Belmabkhout, Y. Versatility vs Stability. Are the Assets of Metal–Organic Frameworks Deployable in Aqueous Acidic and Basic Media? *Coord. Chem. Rev.* **2021**, *443*, 214020. https://doi.org/10.1016/j.ccr.2021.214020.

(46) Gaab, M.; Trukhan, N.; Maurer, S.; Gummaraju, R.; Müller, U. The Progression of Al-Based Metal-Organic Frameworks : From Academic Research to Industrial Production and Applications. *Micro. Meso. Mater.* **2012**, *157*, 131–136.

(47) Alvarez, E.; Guillou, N.; Martineau, C.; Bueken, B.; Van de Voorde, B.; Le Guillouzer, C.; Fabry, P.; Nouar, F.; Taulelle, F.; de Vos, D.; Chang, J.-S.; Cho, K. H.; Ramsahye, N.; Devic, T.; Daturi, M.; Maurin, G.; Serre, C. The Structure of the Aluminum Fumarate Metal–Organic Framework A520. *Angew. Chem. Int. Ed.* **2015**, *54* (12), 3664–3668. https://doi.org/10.1002/anie.201410459.

(48) Jeremias, F.; Fröhlich, D.; Janiak, C.; Henninger, S. K. Advancement of Sorption-Based Heat Transformation by a Metal Coating of Highly-Stable, Hydrophilic Aluminium Fumarate MOF. *RSC Adv.* **2014**, *4* (46), 24073–24082. https://doi.org/10.1039/C4RA03794D.

(49) Yot, P. G.; Vanduyfhuys, L.; Alvarez, E.; Rodriguez, J.; Itie, J.-P.; Fabry, P.; Guillou, N.; Devic, T.; Beurroies, I.; Llewellyn, P. L.; Van Speybroeck, V.; Serre, C.; Maurin, G. Mechanical Energy Storage Performance of an Aluminum Fumarate Metal-Organic Framework. *Chem. Sci.* **2016**, *7*, 446–450.

(50) Férey, G.; Serre, C. Large Breathing Effects in Three-Dimensional Porous Hybrid Matter: Facts, Analyses, Rules and Consequences. *Chem. Soc. Rev.* **2009**, *38*, 1380–1399. https://doi.org/10.1039/b804302g.

(51) Mazouzi, D.; Lestriez, B.; Roué, L.; Guyomard, D. Silicon Composite Electrode with High Capacity and Long Cycle Life. *Electrochem. Solid-State Lett.* **2009**, *12* (11), A215. https://doi.org/10.1149/1.3212894.

(52) Kentgens, A. P. M.; Verhagen, R. Advantages of Double Frequency Sweeps in Static, MAS and MQMAS NMR of Spin I=3/2 Nuclei. *Chem. Phys. Lett.* **1999**, *300* (3), 435–443. https://doi.org/10.1016/S0009-2614(98)01402-X.

(53) Massiot, D.; Fayon, F.; Capron, M.; King, I.; Le Calvé, S.; Alonso, B.; Durand, J. O.; Bujoli, B.; Gan, Z.; Hoatson, G. Modelling One- and Two-Dimensional Solid-State NMR Spectra. *Magn. Reson. Chem.* **2002**, *40*, 70–76.

(54) karmakar, S.; Dechnik, J.; Janiak, C.; De, S. Aluminium Fumarate Metal-Organic Framework: A Super Adsorbent for Fluoride from Water. *J. Hazardous Mater.* **2016**, *303*, 10–20. https://doi.org/10.1016/j.jhazmat.2015.10.030.

(55) Haouas, M.; Taulelle, F.; Martineau, C. Recent Advances in Application of 27Al NMR Spectroscopy to Materials Science. *Prog. Nuclear Magnetic Res. Spectro.* **2016**, *94–95*, 11–36. https://doi.org/10.1016/j.pnmrs.2016.01.003.

(56) Wang, Y.; Qu, Q.; Liu, G.; Battaglia, V. S.; Zheng, H. Aluminum Fumarate-Based Metal Organic Frameworks with Tremella-like Structure as Ultrafast and Stable Anode for Lithium-Ion Batteries. *Nano Energy* **2017**, *39*, 200–210. https://doi.org/10.1016/j.nanoen.2017.06.007.

(57) Wilkes, B. N.; Brown, Z. L.; Krause, L. J.; Triemert, M.; Obrovac, M. N. The Electrochemical Behavior of Polyimide Binders in Li and Na Cells. *J. Electrochem. Soc.* **2015**, *163* (3), A364. https://doi.org/10.1149/2.0061603jes.

(58) Xiong, J.; Dupré, N.; Mazouzi, D.; Guyomard, D.; Roué, L.; Lestriez, B. Influence of the Polyacrylic Acid Binder Neutralization Degree on the Initial Electrochemical Behavior of a Silicon/Graphite Electrode. *ACS Appl. Mater. Interfaces* **2021**, *13* (24), 28304–28323. https://doi.org/10.1021/acsami.1c06683.

(59) Aurbach, D.; Daroux, M. L.; Faguy, P. W.; Yeager, E. Identification of Surface Films Formed on Lithium in Propylene Carbonate Solutions. *J. Electrochem. Soc.* **1987**, *134* (7), 1611. https://doi.org/10.1149/1.2100722.

(60) Aurbach, D.; Moshkovich, M.; Cohen, Y.; Schechter, A. The Study of Surface Film Formation on Noble-Metal Electrodes in Alkyl Carbonates/Li Salt Solutions, Using Simultaneous in Situ AFM, EQCM, FTIR, and EIS. *Langmuir* **1999**, *15* (8), 2947–2960. https://doi.org/10.1021/la981275j.

(61) Meyer, B. M.; Leifer, N.; Sakamoto, S.; Greenbaum, S. G.; Grey, C. P. High Field Multinuclear NMR Investigation of the SEI Layer in Lithium Rechargeable Batteries. *Electrochem. Solid-State Lett.* **2005**, *8* (3), A145. https://doi.org/10.1149/1.1854117.

(62) Delpuech, N.; Dupré, N.; Mazouzi, D.; Gaubicher, J.; Moreau, P.; Bridel, J. S.; Guyomard, D.; Lestriez, B. Correlation between Irreversible Capacity and Electrolyte Solvents Degradation Probed by NMR in Si-Based Negative Electrode of Li-Ion Cell. *Electrochem Commun.* **2013**, *33*, 72–75. https://doi.org/10.1016/j.elecom.2013.05.001.

(63) Dupré, N.; Moreau, P.; De Vito, E.; Quazuguel, L.; Boniface, M.; Bordes, A.; Rudisch, C.; Bayle-Guillemaud, P.; Guyomard, D. Multiprobe Study of the Solid Electrolyte Interphase on Silicon-Based Electrodes in Full-Cell Configuration. *Chem. Mater.* **2016**, *28* (8), 2557–2572. https://doi.org/10.1021/acs.chemmater.5b04461.

(64) Hubaud, A. A.; Schroeder, D. J.; Key, B.; Ingram, B. J.; Dogan, F.; Vaughey, J. T. Low Temperature Stabilization of Cubic (Li7−xAlx/3)La3Zr2O12: Role of Aluminum during Formation. *J. Mater. Chem. A* **2013**, *1* (31), 8813–8818. https://doi.org/10.1039/C3TA11338H.

(65) Camus-Génot, V.; Guiet, A.; Lhoste, J.; Fayon, F.; Body, M.; Kodjikian, S.; Moury, R.; Leblanc, M.; Bobet, J. L.; Legein, C.; Maisonneuve, V. Controlled Morphology Synthesis of Nanostructured β-AlF3–x(OH)x with Tunable Specific Surface Area. *Crystal Growth Des.* **2021**, *21* (10), 5914–5927. https://doi.org/10.1021/acs.cgd.1c00808.

(66) Armand, M.; Grugeon, S.; Vezin, H.; Laruelle, S.; Ribière, P.; Poizot, P.; Tarascon, J.-M. Conjugated Dicarboxylate Anodes for Li-Ion Batteries. *Nature Mater.* **2009**, *8*, 120–125.

Table of Content